Towards a Better Control of Engineered Circuit Transcription in Bacterial Genomes

Nazim Sarica, Laurent Janniere, Brian C Jester

applied microbiology

MDPI

Article

Towards a Better Control of Engineered Circuit Transcription in Bacterial Genomes

Nazim Sarica †, Laurent Janniere * and Brian C. Jester *,‡

Génomique Métabolique, Genoscope, Institut François Jacob, CEA, CNRS, Université Evry, Université Paris-Saclay, 91000 Evry, France

* Correspondence: laurent.janniere@sfr.fr (L.J.); brian@synovance.com (B.C.J.)

† Current address: Institut de Génétique Humaine, UMR 9002 CNRS, 141 rue de la Cardonille, 34090 Montpellier, France.

‡ Current address: Synovance, 104 Avenue George Clemenceau, 94360 Bry Sur Marne, France.

Abstract: The transcription of genes and engineered circuits can deeply vary when inserted into different genomic loci. This unpredictable performance, termed context sensitivity, complicates strain development. Although the causes and mechanisms of context sensitivity are emerging, it is poorly known how to engineer circuits and synthetic pathways isolated from it. Using tools of synthetic biology for designing and inserting various reporter cassettes in the *Escherichia coli* genome and RT-qPCR for directly measuring gene transcription, we first surveyed the genomic landscape for context sensitivity at 214 positions in cells grown in glucose or glycerol. The results show deep variations in cassette transcription with respect to position (up to 160-fold) and growth condition (up to a 30-fold). We then demonstrated that this position-dependent transcription variability is strongly reduced when the reporter cassette is insulated in an artificial protein-bound DNA loop. Finally, we measured the transcription of two loop-insulated genes at different genomic positions. The results show that transcription strongly depends on the relative orientation of the genes, promoter strength, and positive supercoiling. We present a model suggesting that DNA looping is an important cause of context sensitivity and can be used for better controlling the transcription of engineered circuits.

Keywords: *Escherichia coli*; transcription; regulation; context sensitivity; supercoiling; epigenetic; DNA loops; lambda cI

Academic Editor: Ian Connerton

Received: 21 November 2024
Revised: 29 January 2025
Accepted: 5 February 2025
Published: 7 February 2025

Citation: Sarica, N.; Janniere, L.; Jester, B.C. Towards a Better Control of Engineered Circuit Transcription in Bacterial Genomes. *Appl. Microbiol.* **2025**, *5*, 17. https://doi.org/10.3390/applmicrobiol5010017

1. Introduction

Synthetic biology is defined as the design and construction of new biological systems for useful purposes. Advances in this field have been hampered by the unpredictable performance of synthetic circuits and biosynthetic pathways once inserted into the genome. Recent bacterial studies have shown that, depending on the insertion site in the genome, a reporter gene expressed from a single promoter and flanked by transcriptional terminators produces different levels of transcript [1,2]. Although our understanding of this phenomenon, termed 'context sensitivity', is rapidly improving (see below), it is poorly known how to engineer circuits or synthetic pathways that are isolated from it.

Experimental and modeling studies show that a major cause of context sensitivity is the supercoiling induced by the transcription of neighboring genes [3–5]. Importantly, transcription is a major determinant of the supercoiling landscape in bacterial genomes [6], and transcription and supercoiling are mutually influential (reviewed, for instance, in [7–12]).

The interplay between both processes is nicely illustrated by the twin-supercoiled domain model of Liu and Wang [13]. This model, which is extensively supported by both single-molecule studies and genome-wide analysis [6,14,15], posits that RNA polymerase creates negative supercoils upstream and positive supercoils downstream of the sequence it transcribes. These changes can smoothly decay from both sides of the gene of interest and affect the topology of up to 40 neighboring genes. A large core of data show that supercoiling impacts transcription initiation and elongation in different ways [12]. For example, accumulating positive supercoils downstream of transcription forks, a phenomenon termed 'positive supercoiling buildup' (PSB), inhibits transcription initiation and slows down elongation, eventually leading to backtracking, stochastic bursts of expression, and abortive transcription cycles [16]. On the other hand, the accumulation of negative supercoils upstream of the transcription complex generally promotes transcription initiation.

Two types of intermingled processes control genome supercoiling: supercoil removal and supercoil diffusion. Supercoil removal is carried out by topoisomerases. These enzymes maintain supercoiling homeostasis to keep the negatively supercoiled state needed for DNA operations. They reduce either positive or negative supercoils by binding DNA, cutting the phosphate backbone, and either twisting or untwisting the strands before resealing the DNA [17,18]. During transcription, the gyrase, which is the only enzyme that reduces positive supercoiling in the model bacterium *Escherichia coli* [19], removes supercoils downstream of the transcribing RNA polymerase preventing PSB [16,20]. Conversely, Topo I removes the negative supercoils accumulating upstream from the transcription machinery [21].

The diffusion of transcription-induced supercoils is limited by barriers that topologically isolate DNA regions of 10–400 kb in size [22,23]. In other words, gene expression in a given topological region will not impact the topology and transcription in other regions. Several structures can operate as topological barriers. First, the actively transcribing RNA polymerase blocks supercoil dissipation and thus forms a topological barrier [13,24,25]. A similar activity has been assigned to proteins tightly bound to DNA (the bacteriophage λ O initiator protein, the transcription factors LacI and GalR, and the Nucleoid Associated Proteins (NAPs) FIS) [26–28]. Second, during transcription, the RNA polymerase causes torsional stresses to the DNA fiber that self-wrap to form plectonemic structures [14,29,30]. At a larger scale, these dynamic structures organize to form topological barriers [22,23] possibly stabilized by the binding of NAPs like HU, IHF, and FIS to the top or cross-over points of plectonemes [12,31,32]. Finally, supercoiling diffusion is prevented by proteins (NAPs, transcription factors…) forming DNA loops and other long-range 3D arrangements [27,33–35]. In a synthetic biology study carried out on a plasmid-born system, the expression of a gene trapped in a LacI-mediated DNA loop was shown to be insensitive to neighboring gene transcription (e.g., isolated from context sensitivity) and to mainly depend on the promoter strength and its distance to the upstream barrier [36].

The *E. coli* study reported here showed that context sensitivity remarkably varies with the position and growth condition all along the chromosome. It also demonstrated that a gene is efficiently isolated from context sensitivity when embedded in an artificial protein-mediated DNA loop. Finally, our data show that the transcription of two genes within a DNA loop strongly depends on their relative orientation, promoter strength, and positive supercoiling. Altogether, our findings enforce the importance of DNA looping and supercoiling in context sensitivity, and will be of particular interest for synthetic biologists and the engineering of standardized genetic circuits.

2. Materials and Methods

2.1. DNA Sequences

To define the genomic landscape for context sensitivity, we constructed a library of strains that had a single reporter cassette randomly inserted into different genomic locations. The sequences of the initial cassette, as well as that of p3, p10, GRS, nDNA, and *mCherry*, are provided Figure S1. The promoter p1 is from the laboratory collection, while p3 and p10 are described elsewhere [37]. P3 is about 3.5- and 8-fold stronger than p10 and p1, respectively ([37] and this work). Terminator and GRS sequences are from [38–40].

2.2. Plasmid Construction

Plasmids and primers are listed Tables S1 and S2, respectively.

We modified vectors used for Tn10 mutagenesis [41] as illustrated in Figure S2. Briefly, the pNKBOR plasmid was modified so that the RK6 gamma *ori* resides just upstream the transposase gene and would not be incorporated into the genome. All cloning steps for constructs containing the RK6 gamma *ori* were performed using DH5α-pir. A second IS101 site was inserted between the transposase and the kanamycin resistance gene, resulting in pNK2. A synthetic DNA fragment (from IDT-DNA) containing the *emGFP* gene was then ligated into the NotI site of pNK2. The yielded pNK2-827.4 plasmid was validated by sequencing.

To add the DNA binding sites for lambda cI to each side of the reporter cassette, a template vector was constructed for generating PCR products that would be used for lambda red integration. Initially, plasmid pTKIP was modified by swapping the kanamycin cassette with a phleomycin resistance cassette. pTKIP was digested with BamHI and the phleomycin resistance gene (obtained as synthetic fragment from IDT-DNA) was ligated into the corresponding site, resulting in pBCJ879.2. Lambda cI boxes were added to the reporter cassette using PCR on pNK2-827.4 and primers A78F and A78R that contain cI boxes as overhangs. pBCJ879.2 was then digested with KpnI, and the *emGFP* reporter cassette was inserted using the Simply Seamless DNA Assembly Kit (using manufacturer's protocol), resulting in pBCJ932. To express *emGFP* from a strong promoter (p3), we used inverse PCR (primers A115F and A115R) of pBCJ932, resulting in pBCJ927.

To construct a strain of *E. coli* that had the lambda cI protein expressed from the inducible rhamnose promoter, lambda red was used. This required the construction of a plasmid that could be used as a template for a PCR product. The lambda cI gene was purchased as a synthetic DNA fragment from IDT-DNA and inserted into the KpnI site of pBCJ879.2 resulting in plasmid pBCJ937.1.

To construct plasmid β5 carrying the GRS downstream *emGFP*, plasmid pBCJ927 was amplified by inverse PCR using primers N1F and N1R. A synthetic DNA fragment carrying the GRS flanked by 20bp homologous pads to insertion site (from IDT-DNA) was inserted into the plasmid pBCJ927 by ligation (T4 DNA Ligase, NEB), resulting in plasmid β5. Same approach was used for plasmids β9 and β16, using primers N2F and N2R and N3F and N3R, respectively, for inverse PCRs on plasmid pBCJ927.

To construct plasmid β7 carrying the neutral DNA downstream *emGFP*, plasmid pBCJ927 was amplified using inverse PCR and primers N1F and N1R. A neutral DNA product was obtained by amplifying a region from *araD* gene that was manually checked to ensure that it did not contain any known sequence that would interfere with cellular mechanisms (enzyme restriction site, promoter like sequence, ribosome binding site). Primers N6F and N6R, containing overhangs, were used to insert the PCR product in the plasmid backbone by ligation.

To construct plasmid β23, primers N64F and N19R were used to amplify the *mCherry* gene from plasmid pMC48. Primer N64F binds at the beginning of *mCherry* and has an

overhang that contains a random 44 bp sequence (as a replacement for p1 promoter) and a 20 bp sequence homologous to insertion site in backbone plasmid. Primer N19R binds at the end of the *mCherry* gene and carries a terminator and a 20 bp homologous sequence for insertion in the backbone plasmid. Primers N64R and N22R were used to amplify the backbone plasmid from plasmid pBCJ927. The two PCR fragments were then ligated to obtain plasmid β23.

To construct the plasmid β22 carrying emGFP with mutated p3 promoter, plasmid pBCJ927 was amplified by inverse PCR using primers N53F and N53R. These primers carry overhangs containing a replacement sequence for p3 and 20 bp homologous sequences to each other. The PCR fragment was ligated to itself, resulting in plasmid β22.

The plasmid pMC48 was constructed by inserting a DNA fragment purchased from IDT-DNA, encoding a gentamycin resistance gene into pJet2.1.

2.3. Strain Construction

The strains are listed in Table S3, and the used primers are listed in Table S2.

To engineer a strain that has the lambda cI gene expressed from the inducible rhamnose promoter, lambda red recombination was used. PCR of pBCJ937.1 with primers (A143R and A144R) generated a DNA fragment that was used to directly replace the *rhaBAD* genes with lambda cI and a phleomycin resistance marker using lambda red recombineering, resulting in strain BCJ952.4. The phleomycin resistance marker was subsequently removed by lambda red integration of a cassette carrying a neomycin resistance gene, which was then excised from the loci, resulting in α1.

Lambda red integration was used to construct a series of strains that have the *emGFP* gene expressed by the weak p1 promoter flanked by lambda cI binding sites. PCR fragments were generated using pBCJ932 as template and a series of primers that targeted the cassette to different genomic locations. Lambda red genomic integrations were performed as described previously [42,43]. To construct strains 2 to 36, the PCR fragments were integrated into *E. coli* MG1655, and for strains α2 to α23, the PCR fragments were integrated into α1.

We used lambda red to construct strains that have *emGFP* expressed from the strong p3 promoter flanked by lambda cI binding sites. Plasmid pBCJ927 was used as a PCR template to construct strains α28 to α36. To engineer strains α61 to α64, lambda red recombineering was used. PCR reactions using primers 150F-R, 164F-R, 249F-R, and 250F-R were performed on plasmid ß5. These amplifications were then inserted in the target genomic loci using lambda red recombination.

To build strains α66 to α69, PCR reactions using primers 150F-R, 164F-R, 249F-R, and 250F-R were performed on plasmid ß7. These amplifications were then inserted in the target genomic loci using lambda red recombineering.

To build strains α120 to α123, PCR reactions using primers 150F-R, 164F-R, 249F-R, and 250F-R were performed on plasmid ß16. These amplifications were then inserted in the target genomic loci using lambda red recombineering.

To build strains α125 to α150 and α165 to α168, primers N19F, N21F, N23R, N39R, N43F, N46F, and N65R were used to amplify *mCherry* from plasmid 48. When needed, these primers have an overhang containing a replacement sequence for the promoter part. These amplifications were then inserted in the target genomic loci using lambda red recombineering in strains α26 or α36.

To build strains α153 and α154 PCR, reactions using primers 150F-R and 250F-R were performed on plasmid ß22. These amplifications were then inserted in the target genomic loci using lambda red recombineering.

To build strains α169 and α170, PCR reactions using primers N22R and N64R were performed on plasmid ß23. These amplifications were then inserted in the target genomic loci using lambda red recombineering.

To build strains α179 to α184, PCR reactions using primers listed in Table S2 were performed on plasmid ß5, amplifying only the GRS. The PCR product was then inserted in the target genomic loci in strains α129, α131, α149, α150, α167, or α168 using lambda red recombineering.

To build strains α240 to α242 expressing mutants of lambda cI protein, a PCR product containing the chloramphenicol resistance gene amplified from pMC48 using primers N88F-R was inserted in *E. coli* genome, truncating the lambda cI gene. A second PCR product (obtained with primer N84F, N86F, or N92F) containing the P158T, Y210H, or S228R mutation was introduced in replacement for the chloramphenicol resistance gene using lambda red recombineering. Colonies sensitive to chloramphenicol were selected. The sequence of the lambda cI mutants were verified using PCR and sequencing.

The primers and genetic constructs were designed using MacVector software and EcoCyc [44].

2.4. Cell Growth Conditions and Transposon Mutagenesis

Luria Broth (LB) was used for the routine growth of *E. coli* strains. To randomly insert the reporter cassette into the *E. coli* genome, the plasmid pNK2-827.4 was introduced into chemically competent MG1655 cells (the plasmid could not replicate in this host). After 2 h of incubation in LB, the transposed cells were plated on Km LB plates for selecting strains that underwent cassette integration. To identify the site of insertion, the genomic DNA from the selected strains was extracted, restricted, and self ligated. Cassette primers were then used to amplify and sequence the ligated region. M9 media supplemented with glucose or glycerol was used for growing strains for RNA extraction and RT-qPCR measurements. M9 media contains 6 g/L Na_2HPO_4, 3 g/L KH_2PO_4, 0.5 g/L NaCl, 0.002% Casamino acids, 2 mM $MgSO_4$, 100 µM $CaCl_2$, and 0.8% glucose or glycerol as a carbon source. Antibiotics were added to the culture as needed at the following concentrations: spectinomycin (60 µg/mL), kanamycin (25 µg/mL genomic integrations, 50 µg/mL for plasmids), phleomycin (10 µg/mL), gentamicin (10 µg/mL), and ampicillin (100 µg/mL). Bacterial cultures were grown at 30 °C or 37 °C with 200 rpm agitation.

2.5. Molecular Biology Methods

For routine PCR amplification, Q5 and OneTaq DNA Polymerase was used according to the manufacturer's protocol (NEB®, Evry, France). PCR products were cleaned using a Monarch DNA CleanUp Kit and plasmids were purified using a Monarch Plasmid Miniprep Kit, following the manufacturer's protocols (from NEB®, Evry, France). A PureLinkTM Genomic DNA Extraction Kit was used to extract genomic DNA (Thermo Fisher Scientific®, Asnières sur Seine, France). A Simply Seamless DNA Assembly Kit was used to assemble the synthetic DNA fragments, following the manufacturer's supplied instructions Synovance®, Brie sur Marne, France).

Electrocompetent cells were prepared using regular procedures. Briefly, bacterial strains were grown overnight in LB containing the appropriate antibiotics. This seed culture was then diluted 1:400 to inoculate 200 mL of LB containing antibiotics and IPTG if necessary, and grown at 30 °C until reaching OD600~0.5. Cell pellets were harvested by centrifugation at 3900× *g* at 4 °C for 6 min and washed 2 times with an equal volume of ice-cold 10% glycerol and then resuspended in 2 mL 10% glycerol.

Electroporations were performed on an Eppendorf 2510 using manufacturer-supplied protocols. Prior to electroporations performed for lambda red, all PCR fragments were

digested with DpnI for 1 h to remove the template plasmid. An amount of 200 ng of purified DNA fragment containing the linear construct to be integrated was mixed with 50 µL electrocompetent cells in 0.1 cm electroporation cuvettes. Cells were electroporated at 1.8 kV and immediately resuspended in 1 mL LB, incubated, shaking at 200 rpm for 3 h at 30 °C, and 100 µL was plated onto LB containing the antibiotics of interest and incubated at 30 °C overnight. Genomic DNA was extracted from putative colonies, PCR was used to amplify the genomic region of the integration, and all strains were confirmed using sequencing.

Routine agarose gel electrophoresis was conducted in a RunOne Electrophoresis System (Embitec) using a Loading Dye from Thermo Fisher Scientific® (Asnières sur Seine, France), a 1% or 2% agarose gel, and a 1X TBE (Tris, Boric Acid, EDTA) buffer, and it was run for 20 min at 100 V. Gels were stained with Ethidium Bromide (Merck, Saint-Quentin-Fallavier) for RNA and Midori Green (Nippon Genetics, Düren, Germany) for DNA, before being visualized under UV light or by using a G-box iChemi (Syngene, Cambridge, UK).

2.6. RNA Isolation

Cells were inoculated to 300 µL M9 Glycerol media and grown overnight at 37 °C. The following day, 10 mL of M9 Glycerol was inoculated with 200 µL of overnight culture. 10 mM Rhamnose was added to the cultures that required expression of lambda cI. The samples were grown until they reached OD600~0.55 and were harvested by centrifugation, 10 min at 3900× *g* at 4 °C. The pellets were snap-frozen in a dry-ice/ethanol bath and stored at −80 °C until the RNA was extracted. To extract the total RNA, cell pellets were transferred to ice and resuspended in 1 mL of Ribozol RNA Extraction Reagent (VWR). RNA extraction was performed according to the manufacturer's supplied protocol. The final RNA pellets were resuspended in approximately 225 µL of water, depending upon pellet size. RNA was treated with DNase I (NEB) according to the company-supplied protocol. RNA was then precipitated by adding of 20 µL sodium acetate and 500 µL isopropanol. RNA was then pelleted at 21,130 g for 30 min, washed in 500 µL of 75% ethanol, and resuspended in 80 µL water. The integrity, quality, and quantity of the purified RNA was determined using agarose gel electrophoresis and nanodrop measurements.

2.7. Reverse-Transcription and Quantitative PCR (RT-qPCR)

Five hundred nanograms of RNA was used to perform Reverse Transcription using a Protoscript II RT Kit according to the manufacturer's supplied protocol (New England BioLabs®, Evry, France). While conducting this large RT-qPCR study, we discovered that there is a significant batch-to-batch variation in Reverse Transcriptase. To prevent this from impacting our datasets, all of the RT-qPCR reagents used during the entire study came from a single production batch. cDNA samples were purified using a GeneJET PCR Purification Kit (Thermo Fisher Scientific® (Asnières sur Seine, France)) and eluted in 50 µL final volume. cDNA samples were diluted 10 times, and qPCR was performed using SYBR Premix Ex Taq Kit (Takara, Kusatsu, Japan), according to the manufacturer's supplied protocol. The primers used to quantify transcription for the different genes are in Table S2. Quantitative PCR was performed on Realplex^2 Mastercycler from Eppendorf® (Montesson, France) using the manufacturer's supplied protocol and the following optimized parameters: 40 cycles with denaturation 5 s at 95 °C, primer annealing for 30 s at 60 °C, and extension at 72 °C for 20 s. An external standard (a dilution series for the corresponding PCR product) was added to each qPCR plate. All samples were measured in duplicate on the plate. All measurements were the average of a minimum of three independent cultures. The standard error was less than 30% for all averaged values.

2.8. Statistics and Data Analysis

Absolute quantification of gene targets was performed via a standard DNA curve. Data analysis was carried out using Microsoft Excel. To obtain the number of transcript per cell, we used the following formula:

$$\text{Number of copies} = (\text{X nanograms} \times \text{Avogadro's number})/(\text{molecular weight} \times 1 \times 10^9)$$

X corresponds to the amount of amplicon generated by qPCR, Avogadro's number (6.0221×10^{23}) corresponds to the number of molecules per mole, molecular weight is 233,703.9 for *emGFP*, and 231,269.38 for *mCherry*, which is multiplied by 1×10^9 to obtain the number of molecules per nanogram of total RNA. This number is then divided by 10,000 to obtain the number of molecules per cell [45,46]. Statistic data were computed using the Mann–Whitney U-test with a significance level of 0.01 and the two-tailed hypothesis (https://www.socscistatistics.com/tests/mannwhitney/default2.aspx; accessed on 6 February 2025).

3. Results

3.1. Context Sensitivity of Transcription in Glucose and Glycerol All Along the E. coli Chromosome

To obtain a global view of context sensitivity within the *E. coli* chromosome, we undertook a transposon mutagenesis approach to randomly insert a transcription reporter cassette throughout the genome. This 1.2 kb reporter cassette has expression of *emGFP* driven by a weak promoter (p1). It also has transcriptional terminators both upstream and downstream of *emGFP* to prevent unwanted transcriptional read-through from flanking genomic regions (Figure 1A, inserted diagram). We confirmed that *emGFP* transcription is indeed derived from the weak promoter and not from read-through transcription using RT-qPCR (Figure S3). The genomic locations for the transposon insertion sites were determined by sequencing. The final library consists of 214 strains that harbor the *emGFP* reporter cassette at unique locations covering the entire genome. Given the tight relationship between growth, genome expression, and genome architecture (see above), and that up to 20% of the genome can be differently expressed in glucose and glycerol [47–50], we investigated how changes in position and growth conditions impact context sensitivity. To that end, the transcription of the *emGFP* reporter cassette was assessed using RT-qPCR in cells grown in media containing either glucose or glycerol as the sole carbon source.

Data plotting showed a clear variation in transcription with respect to position in both carbon sources (Figure 1A, main panel). The mean variability and maximum fold-change were 3.2 and 161 in glucose and 1.9 and 39 in glycerol, respectively. Interestingly, the nutritional conditions differently impacted the position effect on transcription. Changes were either positive or negative: 2.14-fold in average, varying up to 29-fold. In 44% of the positions, transcription varies more than 2-fold (p-value < 0.00001, Mann–Whitney U-test). These results are consistent with a previous study carried out at four genomic positions and in five different media [51]. Surprisingly, the global level of transcription is significantly higher in glycerol (0.0111 +/− 0,0029 TPC) than in glucose (0.0062 +/− 0.0032 TPC) (p-value: <0.00001, Mann–Whitney U-test) (Figure 1A, right panel).

In order to determine whether DNA replication impacts transcription, we compared the library results with the gene dosage of exponentially growing cells. In glucose, the gene dosage is 4 at the replication origin *oriC* and decays progressively to 2 at the replication terminus *terC*, giving a ratio origin sequences/terminus sequences of 2 (Figure 1, green doted line) [52]. In cells that grow slower, like in glycerol [53], the gene dosage and the ratio origin sequences/terminus sequences are lower [54]. When we compared the mean transcription level in 1 MB regions encompassing *oriC* and *terC* (Figure S4), ratios of TPC *oriC*/TPC *terC* of 2.1 in glucose and 1.3 in glycerol were found. As these ratios

are close to the expected origin sequences/terminus sequences ratios, they suggest that DNA replication impacts the transcription profile of Figure 1A in both carbon sources. Consistently, a signal decay from *oriC* to *terC* for both chromosome arms is barely visible in the figure. Despite the global effect of replication on transcription levels, the gene dosage does not affect transcription variability, as the data are similarly dispersed at the *oriC* and *terC* regions (Figure S4).

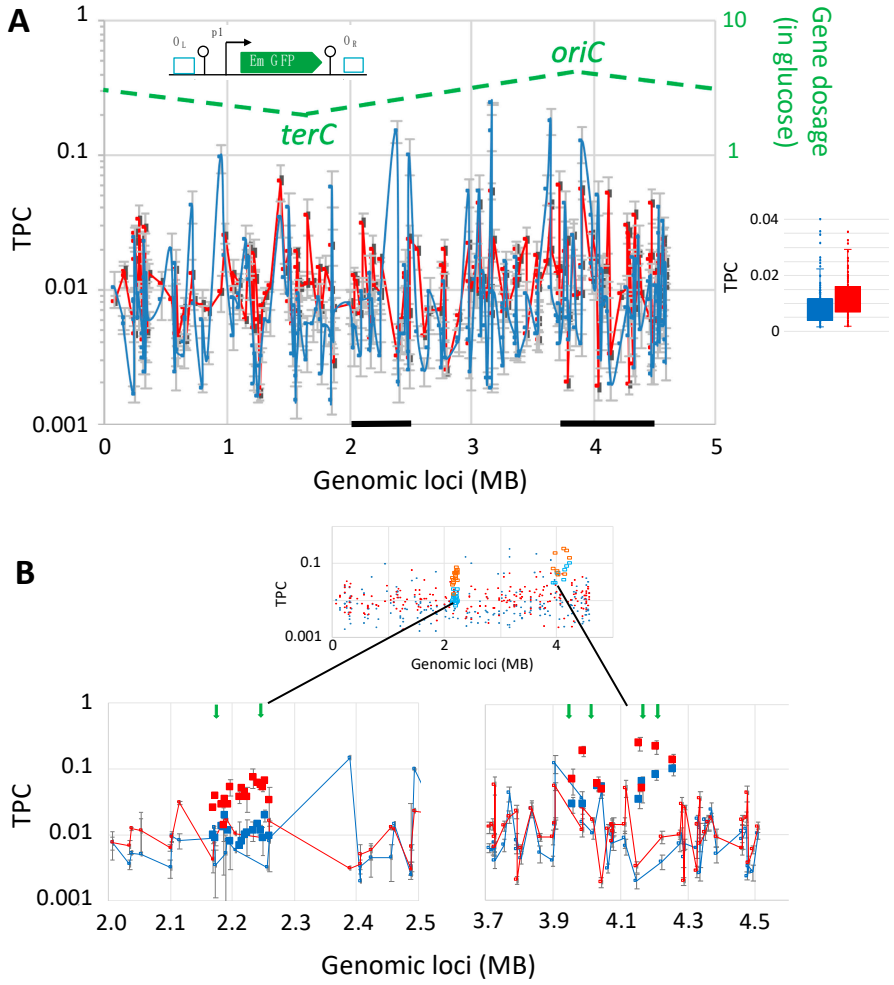

Figure 1. Transcription level of the *emGFP* reporter cassette all along the *E. coli* genome. (**A**) Transcription of the reporter cassette inserted by Tn10 transposition. Tn10 transposition was used to generate 214 strains containing a single copy of the *emGFP* cassette at different positions all along the chromosome. Each strain was grown in minimal media containing either glucose or glycerol as the sole carbon source, and RT-qPCR was used to quantify cassette transcription. Main panel: transcription data plotted as transcripts per cell (TPC) on the *y*-axis vs. genome location on the *x*-axis. Blue and red open squares pinpoint the transcript levels in glucose and glycerol, respectively. Bars stand for standard errors. The dotted green line represents the expected gene dosage for cells growing exponentially in glucose [52]. The thick black lines highlight the regions where non-mutagenic constructs were generated (see panel (**B**)). The histogram on the right of the main panel compares the transcription variability in glucose (blue) and glycerol (red). The 1.2 kb long reporter cassette is diagrammed in the top left corner. The green arrowed box, bent arrow, lollipops, and blue boxes stand for the *emGFP* open reading frame, p1 promoter, transcription terminators, and the left and right lambda cI binding sites. (**B**) Transcription of the reporter cassette at non-mutagenic sites in the Ori and Ter region. Top panel: Genome-wide comparison of the mutagenic and non-mutagenic data. Bottom panels: Zoom-in of both sets of data in regions encompassing the Ori and Ter regions. Non-mutagenic data are represented by large closed squares using the color code of panel **A**.

To determine whether the transcription variability in the library is biased by mutagenic effects caused by transposon insertion (78% of the Tn insertions interrupt open reading frames and are thus potentially mutagenic; see Table S4 for details), we next inserted our reporter cassette at positions rationally curated to be non-mutagenic (e.g., between open reading frames carried by distinct transcription units and between known regulatory features). The insertion sites were located in the Ori and Ter regions. This analysis will help to test whether context sensitivity is uniform throughout the genome or varies in some regions in response to, for instance, local expression level and genome organization (the Ori region is highly expressed and organized by MaoP/*maoS* whilst the Ter region is weakly expressed and organized by MatP/*matS* [55,56]). Eight positions in the Ori region and 17 in the Ter region were thus selected (Figures 1B and S5). The insertion density in the 100 kb long Ter region was intentionally rather high (every 5.7 kb in average) to evaluate how context sensitivity responds at a fine scale.

When results at non-mutagenic sites are sur-imposed onto the library plot (Figure 1B: top panel), it appears that transcription variability is similar for both sets of constructs in glucose and glycerol. This indicates that the library variability is not due to mutagenesis. Interestingly, differences in transcription levels in sub-areas of both the Ter and Ori regions were found. In the Ter region, the transcription level of mutagenic and non-mutagenic constructs between the positions from 2.17 to 2–25 MB is higher in glycerol than in glucose (Figure 1B, left panel), and this difference is highly significant according to the Mann–Whitney U-test (p-value < 0.00001). Interestingly, a transcriptomic study from F. Blattner's lab showed that two operons (*gatZABCD* and *mglAC*) in this sub-area are also more expressed in glycerol than in glucose [57] (Figure S6, generated using the GEO platform (https://www.ncbi.nlm.nih.gov/geo/query/acc.cgi?acc=GSE2037, accessed on 6 April 2025)). Their genomic position is shown Figure 1B (left panel, green arrows). Given that increases in the local concentration of RNA polymerase have been proposed to be a basic principle of transcriptional control [58], it is possible that glycerol-mediated operon inductions in the sub-area of the Ter region result in a local increase in RNA polymerase concentration and basal expression level. In the Ori region, a similar reasoning may apply to two sub-areas (coordinates from 3.91 to 4.05 MB and from 4.16 to 4.26 MB) encompassing each two rrn operons (Figure 1B, right panel, green arrows). The transcription level of both mutagenic and non-mutagenic constructs in these two areas is significantly higher (p-value < 0.0009, Mann–Whitney U-test) than in the remaining areas of Figure 1B (right panel) in both glucose and glycerol. Consistently, broad regions of high transcriptional capacity centered on the ribosomal RNA operon and core metabolic genes have been detected previously [2].

Collectively, our findings confirm the importance of context sensitivity on transcription and suggest that context sensitivity strongly depends on the genome architecture and genome expression pattern imposed by carbon sources. They also show that changes in context sensitivity are obvious even at very close (2–3 kb apart) positions and that context sensitivity is not sensitive to gene dosage, at least at moderate replication rates.

3.2. Transcription in a Protein-Bound DNA Loop Is Protected Against Context Sensitivity

Considering that supercoiling is a major cause of context sensitivity and that supercoiling diffusion is prevented by DNA looping [26,33–36], we decided to evaluate the impact of looping on context sensitivity. To insulate our reporter cassette within a small loop in vivo, we used the lambda cI protein. This protein is known to efficiently bind specific DNA sequences (O_R and O_L) and self-dimerize to form a protein-bound DNA loop in vivo [59–62]. To express lambda cI, we engineered a strain that has, in its genome, the corresponding gene under the transcriptional control of the rhamnose inducible promoter. We confirmed

that this strain expressed lambda cI in the presence of rhamnose using Western blot analysis (Figure S7). To allow for *emGFP* insulation in a loop, the reporter cassette was flanked by the lambda cI binding sites (Figures 1 and 2). The impact of looping on *emGFP* transcription was then investigated in sixteen of the non-mutagenic insertion sites (eight in the Ori region and eight in the Ter region). The corresponding strains were constructed by transferring the reporter cassettes into the lambda cI expressing strain (α1). Transcription of *emGFP* was then quantified using RT-qPCR for strains grown in a medium containing glycerol as the carbon source and rhamnose as the inducer of DNA-loop formation.

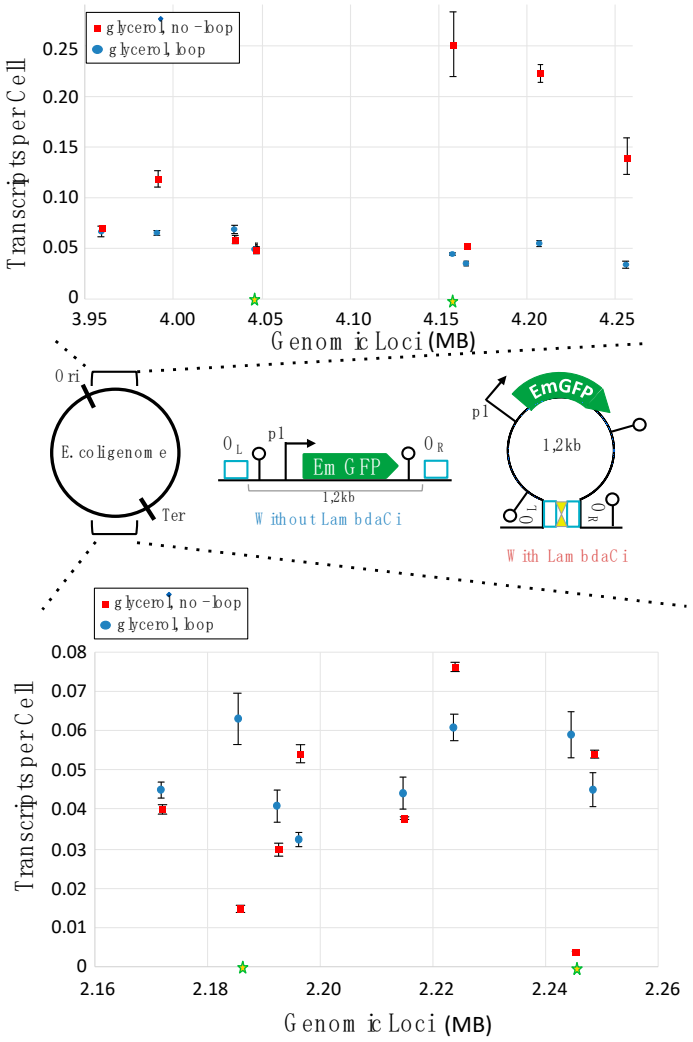

Figure 2. The impact of DNA looping on gene transcription. Transcription levels were quantified using RT-qPCR for the different strains grown in media containing either glycerol (red square, no-loop) or glycerol and rhamnose (blue dots, loop). *x*-axis represents the genomic loci where the constructs have been inserted. *y*-axis represents emGFP TPC. The green stars on the *x* axis represent the genomic loci used for the next experiment. A diagram of the reporter construct is shown in Figure 1. In the presence of the lambda cI protein (yellow triangles), a 1.2 kb DNA-loop is formed.

In condition of loop formation, *emGFP* transcription in both the Ori and Ter regions averages at 0.05 TPC (sd 0.01 TPC), with a maximal variability of 2.1 (Figure 2). Although the un-looped data average at a similar value (0.08 TPC), they vary much more, with a maximal fold-change of 66. Moreover, depending on the position, loop formation is associated with either a transcription increase or decrease compared to the un-looped constructs. These data show that the incorporation of our reporter cassette within a DNA

loop homogenizes p1 expression levels, significantly reducing the transcription variability found in the un-looped configuration.

To further characterize the impact that DNA looping has on transcription, we quantified a series of reporter constructs in which the weak p1 promoter was replaced by the strong p3 promoter (Figure 3a,b). The promoter swapping was carried out in four strains (two harboring the cassette at the Ori region, and two at the Ter region) (loci highlighted by stars in Figure 2). These insertion sites were selected based on the results obtained with the p1 promoter. Sites 2,185,490 and 2,244,773 were selected because loop formation strongly increased transcription (about 5-fold). The insertion site 4,158,229 was selected because loop induction strongly decreased expression (about 5-fold), and site 4,046,827 was chosen because the loop did not appear to have a significant impact on transcription. Expression levels for the p3 constructs were quantified for cells grown in glycerol with or without rhamnose (e.g., with or without a DNA loop, respectively).

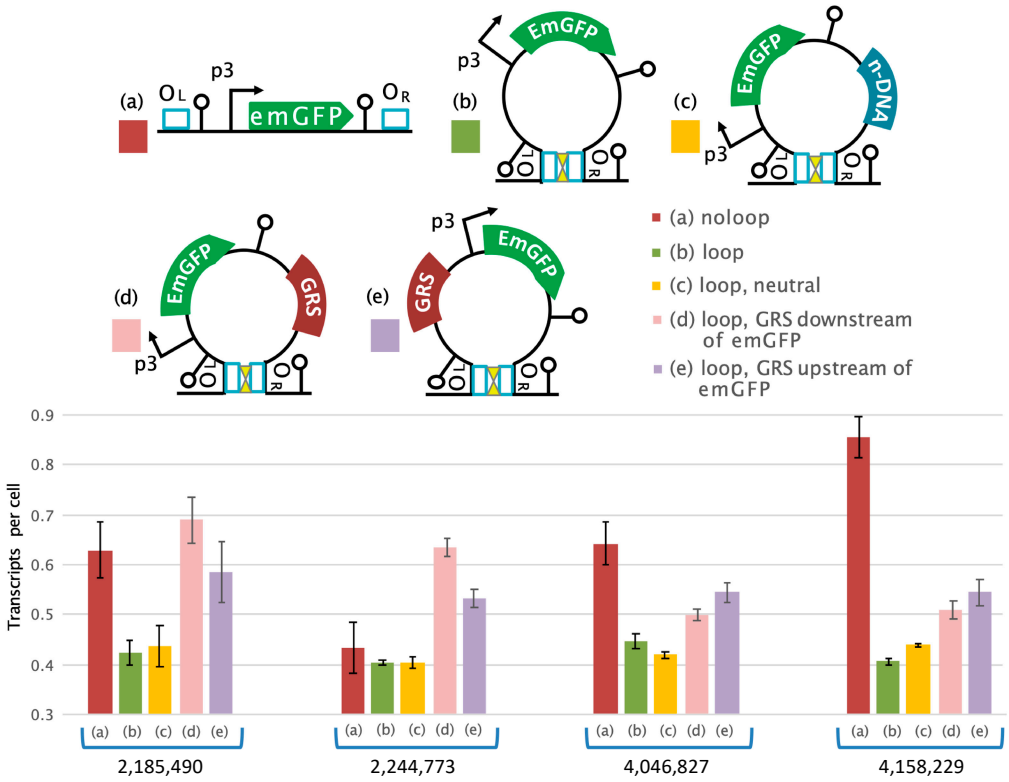

Figure 3. emGFP transcription from the strong p3 promoter in different loop contexts and at four unique genomic positions. Gene transcription was quantified using RT-qPCR for the different strains grown in media containing glycerol and rhamnose. The loop contexts are diagrammed as in Figure 2, with the blue box standing for neutral DNA and the brown boxes standing for GRS: (**a**) initial un-looped cassette; (**b**) initial looped cassette (1.2 kb); loops containing a neutral DNA sequence downstream of emGFP (**c**) or a GRS downstream (**d**) or upstream (**e**) from emGFP (1.4 kb). In the histograms, the *x*-axis stands for the four genomic positions and the *y*-axis stands for TPC.

In the un-looped version, the p3 promoter produces an average of 0.64 TPC ranging from 0.42 to 0.85 TPC, while a nearly constant transcription level (from 0.40 to 0.44 TPC) was found in the looped configuration (Figure 3a,b). This result suggests that strong promoters are less sensitive to the genomic context than weak promoters (the context sensitivity impacts 2-fold p3 and 66-fold p1) and that p3 is, on average, 8-fold stronger than p1 in looped and un-looped configurations. DNA looping seems to also impact the weak p1 and strong p3 promoters differently. While looping increases, decreases, or keeps unchanged

p1 transcription, it mainly decreases p3 activity (in one position, however, it keeps p3 activity unchanged).

Collectively, our results show that the transcription of a gene embedded in a protein-bound DNA loop is effectively protected from the local positive or negative effects of context sensitivity, reaching a homogeneous level at any chromosomal positions. This insulation likely results from the ability of protein-mediated DNA loops to operate as topological barriers that prevent local supercoiling to interfere with gene transcription within the loop. The distinct response of weak and strong promoters to DNA looping may have two main causes: (i) weak promoters are more sensitive to context sensitivity than strong promoters (compare Figures 1 and 2 vs. Figure 3a); (ii) the twin-supercoiled domain and our results (Figure 2 vs. Figure 3a,b) suggest that transcription-induced supercoiling in looped structures more drastically impedes strong rather than weak promoters.

3.3. Reducing the Positive Supercoiling Buildup (PSB) in DNA Loops Increases Transcription Levels

Transcription and supercoiling are mutually influential, and supercoils generated between two topological barriers (e.g., in a protein-mediated DNA loop) cannot escape the insulated region (see above). Hence, the supercoiling generated during *emGFP* transcription in the looped constructs may affect its expression. For highly expressed genes, such interference reduces gene expression. Chong et al. showed that this inhibition is caused by PSB generated by the transcribing RNA polymerase and can be alleviated by the gyrase which relaxes PSB [16]. To investigate the role of PSB on p3-driven *emGFP* transcription in looped constructs, we used a DNA sequence of the Mu-prophage that *E. coli* DNA gyrase recognizes efficiently to relax supercoiling [40]. This sequence, named GRS, was inserted upstream or downstream of *emGFP* (Figure 3d,e), and the synthetic constructs were introduced into the four genomic loci highlighted in Figure 2. As a control, we constructed an isogenic strain that contained downstream of the reporter cassette, a neutral DNA (n-DNA) segment similar in size (~250 bp) to the GRS sequence (Figure 3c). The results show that insertion of a ~250 bp neutral sequence within the original loop does not significantly change *emGFP* transcription, whilst this transcription is increased from 20 to 60% in variants containing the GRS either upstream or downstream from the reporter gene. Overall, these results suggest that reductions in PSB accumulation inside loops increase gene transcription.

3.4. Transcription Levels for Two Genes Within a DNA Loop Strongly Depends on Their Relative Orientation and Promoter Strength

Gene transcription in natural genomes depends on the combined effects of intragenic regulatory determinants (promoter sequence, binding of transcription factors to operators…) and intergenic mechanisms depending on the genome layout (spatial arrangement and orientation of genes), PSB and transcriptional interference [3,63,64]. The level to which intergenic signals contribute to gene transcription control is still unclear. To investigate this issue, we used our synthetic biology approach to test the mutual impact that two transcribed genes have on their transcription in looped constructs. To that end, we inserted, in the cassette containing p3-*emGFP* flanked by the lambda cI binding sites (Figure 3a,b), a second reporter gene (*mCherry*) in three different configurations (Figure 4, top panel): (a) tandem—transcription is co-oriented; (b) convergent—the two genes transcribe into each other; and (c) divergent—transcription proceeds away from each other. These constructs have *mCherry* expressed from the weak p1 or a moderate (p10) promoter (note that p3 is about 3.5- and 8-fold stronger than p10 and p1, respectively (see [37] and above)). Both genes are directly followed by a strong terminator to prevent read-through transcription and transcription fork collisions. The constructs were then inserted into two different

genomic locations (Ori and Ter regions) in the strain expressing lambda cI (α1) and were analyzed in loop formation conditions.

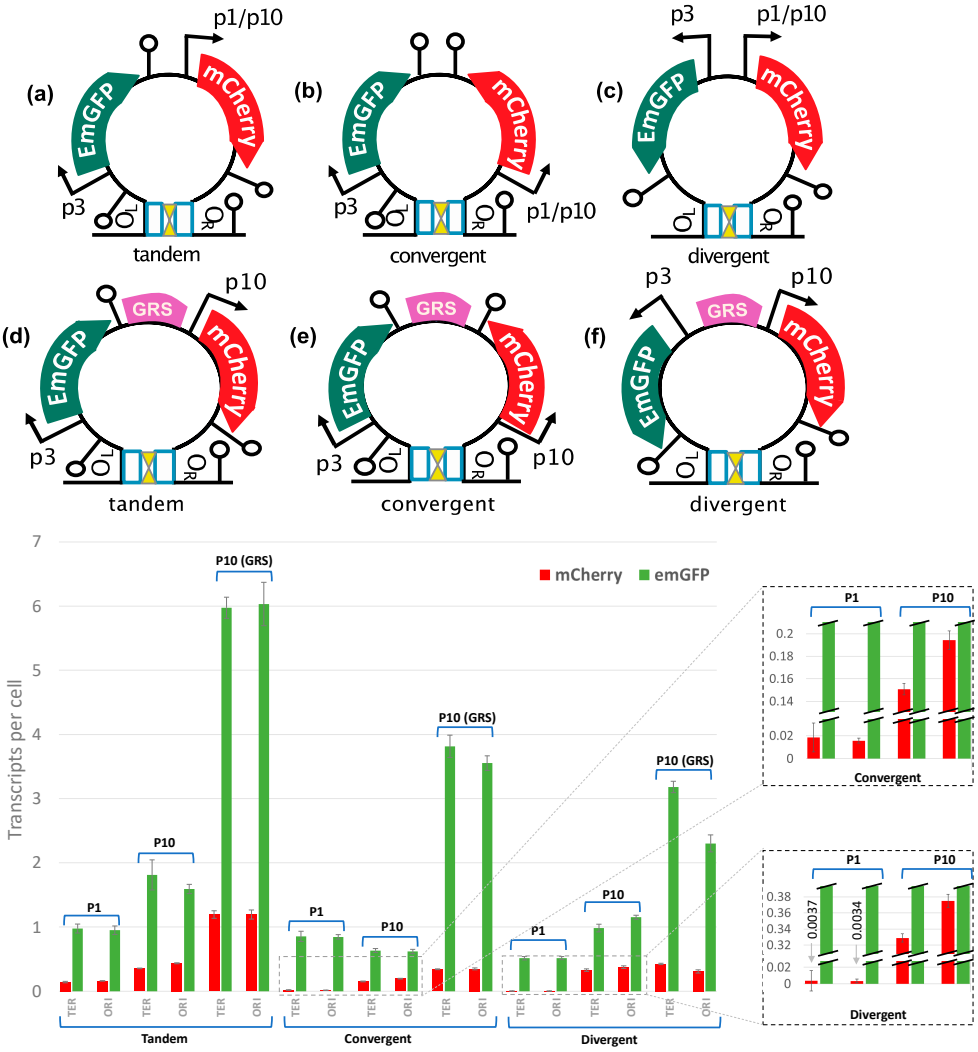

Figure 4. Transcription of *emGFP* and *mCherry* within a DNA loop containing or not containing GRS. Transcription levels were quantified using RT-qPCR for the different strains grown in media containing glycerol and rhamnose. *x*-axis identifies the two genomic regions where the constructs have been inserted, and the *y*-axis represents the number of TPC. The constructs are diagrammed as in Figure 2, with the green and red arrows representing *emGFP* and *mCherry* genes, respectively. Loops with and without GRS are 2.4 and 2.1 kb long, respectively. All constructs have *emGFP* under the control of a strong promoter (p3) and mCherry under control of a weak promoter (p1) or a strong promoter (p10). Tandem: genes transcribed in same orientation. Convergent: genes transcribed in convergent orientation. Divergent: genes transcribed in divergent orientation. p1 bar graphs: *emGFP* under control of p3 and *mCherry* under control of p1. p10 bar graphs: *emGFP* under control of p3 and *mCherry* under control of p10. p10 (GRS) bar graphs: *emGFP* under control of p3, presence of GRS in the intergenic region and *mCherry* under control of p10. Convergent and divergent data for the p1 and p10 constructs are zoomed in to better visualize the weak transcription levels of *mCherry*.

When compared to the original p3-*emGFP* loop construct (about 0.4 TPC, Figure 3b), the insertion of p1-*mCherry* doubled *emGFP* transcription in the tandem and convergent constructs, while it had no effect on the divergent configuration (Figure 4 diagrams a–c and p1 bar graphs) (a *t*-test showed that most of the values in Figure 4 are statistically different (Table S5)). In contrast, the p1-driven transcription of *mCherry* in the tandem configuration is 2-fold lower than in the p1-*emGFP* loop (0.04 vs. 0.02 TPC, respectively; compare Figure 2

(looped data) and Figure 4, diagram a and bar graph p1 in tandem) and further decreases in the convergent (about 9-fold) and divergent (40-fold) constructs. To define how a stronger promoter within the DNA loop impacts transcription, we swapped the weak p1 promoter of *mCherry* with the moderate p10 promoter and quantified transcription for both genes (Figure 4 diagrams a–c and p10 bar graphs). Comparing the *emGFP* transcription profiles for the p1 and p10 constructs, we see that the use of a moderate promoter for *mCherry* nearly doubles *emGFP* expression levels for the tandem and divergent configuration and slightly decreases transcription in the convergent construct (Figure 4 p1 and p10 bar graphs). When mCherry transcription from p10 and p1 are compared, the p10 results show, instead of the dramatic tandem > convergent > divergent decrease in p1 transcription, a relatively high level of activity in the tandem and divergent configurations that is only 2.3-fold reduced in the convergent construct.

Overall, our results show that transcription in DNA-loops containing two genes depends on both the relative gene orientation and promoter strength. Strongest phenotypes were found in constructs containing a weak and a strong promoter. In these situations, the activity of the weak promoter strongly (up to 40-fold) depends on the layout, while that of the strong promoter varies only 2-fold and remains high. In constructs containing a moderate and a strong promoter, the activity of both promoters remains high, and gene orientation impacts transcription from only 2- to 4-fold. Together, these results show that the conformation giving the highest performances for both genes is the tandem layout. We inferred from this that intergenic mechanisms play an important role in gene regulation in topologically insulated DNA sequences and that weak promoters are much more sensitive to these mechanisms than strong promoters.

3.5. PSB Strongly Impacts Transcription Levels for Both Genes Within a DNA Loop

To test the contribution of PSB in gene regulation by intergenic mechanisms, GRS was inserted between the highly transcribed p3-*emGFP* and p10-*mCherry* (Figure 4, diagrams d–f), and mRNA levels were compared to the isogenic constructs lacking GRS (Figure 4, compare bar graphs P10 and P10 (GRS)). Insertion of GRS increased *emGFP* transcription in all orientations (from 3- to 7-fold) and increased *mCherry* expression (2–3-fold) in the tandem and convergent configurations, while having no effect on *mCherry* transcription in the divergent construct. This result suggests that PSB is an important determinant of gene regulation by intergenic mechanisms in loops containing two highly expressed genes. The tandem oriented construct with the GRS produced the highest transcription levels for both genes.

3.6. DNA Loop Formation Is Required for Isolating Transcription from the Genomic Context

Lambda cI is a highly characterized DNA-loop-forming protein. The capacity of this protein to tether distant regions is provided by its ability to bind to DNA operators and self-oligomerize. In the tetrameric form, lambda cI binds operator sequences named O_L and O_R. The interaction between the two tetramers forms an octamer, and this results in the formation of a DNA loop [59–62]. To confirm that DNA loop formation and not solely DNA binding is required for transcriptionally isolating gene expression from the genomic context, we engineered three strains, each expressing a different mutant of lambda cI protein (P158T; Y210H; S228R). These mutants have been well-characterized previously [65]. Two mutations impact the oligomerization ability of lambda cI (P158T; S228R), and the third reduces the capacity of lambda cI to bind adjacent operator sites (Y210H). Briefly, these mutations allow for lambda cI to bind DNA, but prevent the formation of DNA loops.

The (p3-*emGFP*)-GRS-(p10-*mCherry*) construct (tandem configuration) was inserted into strains expressing one of the three lambda cI mutants. The results show that transcrip-

tion levels for both *emGFP* and *mCherry* are similar in cells lacking the lambda cI protein and in strains producing a mutated cI form (Figure S8). These results confirm that the formation of a DNA loop is required for transcriptional insulation of the cassette from context sensitivity.

4. Discussion

Our work investigates the cause of context sensitivity using a synthetic biology approach. As a first step, we obtained an overview of the genomic landscape for this phenomena using a library of 214 strains (Table S4) that harbor the *emGFP* reporter cassette at unique locations, covering the entire genome. Previously, different groups have taken similar approaches, where they quantitated expression levels of a reporter gene that was placed at different genomic locations. These studies generally quantitated expression levels for strains grown in a single growth condition, providing a static snapshot of transcription variability. In our study, we accurately measured reporter transcription in the library in two growth conditions that significantly change (up to 20%) chromosome expression [47–50] and are thus assumed to alter genome architecture [9,11]. This gave us the unprecedented opportunity to obtain a dynamic view of how two different chromosomal conformations influence transcription of the exact same reporter construct genome-wide. Additionally, previous studies often used strong promoters to drive the expression of the reporter gene. We demonstrated that a gene expressed from a weak promoter is more sensitive to the influence of its genomic context and used such a promoter for our genome-wide study. Other studies have used fluorescence to track transcriptional responses. Although this is an easy way to obtain expression data, we believe that by quantitating the protein end-product, the results could be misleading due to other factors that influence final protein levels (post-transcriptional regulation, translational and post-translational regulation, maturation/stability of the fluorophore, translational loading, and competition for translational proteins). For this reason, we used RT-qPCR to determine transcription levels, one of the most accurate methods for mRNA quantification.

Our report confirms that context sensitivity has a remarkable influence on transcription all along the chromosome (Figure 1) [2]. This effect can be quite different even at close (2–3 kb) positions, and it is insensitive to gene dosage. This study also further supports the fact that context sensitivity is influenced by the transcription of neighboring genes [2]: higher local levels of cassette transcription were found in ~100 kb long regions encompassing strong *rrn* operons or metabolic operons (*gatZABCD* and *mglAC*) induced in glycerol [57]. Given that increases in the local concentration of RNA polymerase have been proposed to be a basic principle of transcriptional control [58], it is possible that the basal level of transcription locally increases at the vicinity of highly transcribed genes.

This work clearly shows, in addition, that context sensitivity responds quite noticeably to nutritional conditions. At the genome level, transcription of the reporter cassette was 1.8-fold (p-value < 0.00001) higher in glycerol than in glucose. At the position level, carbon sources alter cassette expression either positively or negatively at the majority of positions, the effect being >2-fold at 44% of the positions (p-value < 0.00001). As the major causes of context sensitivity are the supercoiling induced by transcription and protein-DNA interactions that form barriers to supercoil diffusion, the cellular physiology afforded by glucose and glycerol seems to alter genome transcription and architecture to a level sufficient for impacting context sensitivity genome-wide.

To understand the impact that topological domains have on context sensitivity, we used the lambda cI protein to incorporate the *emGFP* reporter cassette within a DNA loop (Figure 2). We found that the *emGFP* transcription is homogenized when incorporated within a loop, significantly reducing strain-to-strain variability. The control experiments

using lambda cI mutants demonstrate that this effect depends on DNA loop formation. It is, however, important to note here that cI-mediated DNA loops can be destabilized by transcribing RNA polymerases [66]. To prevent such interferences, transcription terminators were cloned inside the loop at the 5′ and 3′ ends of *emGFP*, and most (10/16) of the constructs were inserted in non-transcribed regions (e.g., between the transcription terminator of a gene and the promoter of the downstream gene). However, transcription forks from upstream or downstream promoters may enter the looped region in six remaining strains (in these cases, the cassette was inserted few nucleotides downstream from an ORF or in a region containing "secondary" promoters). As the (potentially) transcribed and non-transcribed constructs gave similar results (e.g., high variability in the un-looped configuration and transcription homogenization in the looped configuration, Figure S9), elongating RNA polymerases from external promoters do not seem to significantly destabilize cI-mediated DNA loops in our study. Differences in transcription rates from external promoters may explain the apparent discrepancy between the two studies. In our work, these rates would be too low to significantly destabilize the loops and abrogate their effect on context sensitivity. In agreement with previous findings [27,33–36], we thus propose that the loop-induced protection from context sensitivity results from the ability of protein-forming loops to operate as topological barriers that prevent local supercoiling to interfere with gene transcription within the loop. The use of DNA loops can thus be extremely beneficial for synthetic biology projects, as it increases the predictable performance of synthetic circuits and biosynthetic pathways once inserted into the genome. It should, however, be kept in mind that our study focus on $\leq$2.5 kb loops while natural loops range 10–400 kb in size (see above). However, it was recently shown that all active transcription units form discrete topological barriers [25]. As the *E. coli* genome encompasses about 4000 transcription units [67], small loops of the size range of the synthetic loops investigated here may spontaneously form in *E. coli*.

In the looped configuration, the expression of strong promoters is often lower than in the un-looped version. We showed that this is due to PSB accumulation by introducing a GRS site inside the loops. In loops containing two genes, this insertion increased transcription up to 700% compared to the same construct without GRS. These observations suggest that PSB is an important determinant of context sensitivity and that GRS is a potent tool to improve gene transcription within a loop.

To further characterize transcription within a protein-bound DNA loop, we introduced, in different relative orientations, a second gene expressed by a weak or moderate promoter (Figure 4). The tandem gene orientation gave the highest transcription levels for both reporter genes. According to the twin-supercoiled domain model, we would expect the positive supercoils produced during transcription of the upstream *emGFP* gene to be countered by the negative supercoils induced by transcription of the downstream *mCherry* gene. This decrease in topological constraints in the intergenic region could be beneficial for the transcription of both genes. For *emGFP*, it would reduce the negative effects of PSB. For *mCherry*, it would facilitate the recruitment of the RNA polymerase at the promoter and/or its transition to the open complex.

In the convergent orientation, the transcribing RNA polymerases are expected to increase PSB in the intergenic region and impede the transcription of both genes. Consistently, when comparing data from the weak and strong promoter for *mCherry*, we found that an increase in mCherry transcription results in a decrease in emGFP transcription. Moreover, the transcription of both genes is strongly stimulated when PBS is reduced by inserting GRS in the intergenic region. Interestingly, in the absence of GRS, a ~0.2 TPC increase in mCherry results in a ~0.16 TPC decrease in emGFP. This observation suggests that a limited quantity of PSB is tolerated between these two genes and that the total transcripts for this

configuration are partitioned between the two genes based upon relative promoter strength. In a recent work, Bryant et al. also observed the mutual negative impact of convergent transcriptional units in the *E. coli* chromosome [1]. Overall, these observations strongly suggest that the transcription of convergent genes impede each other.

We additionally observed that, when *mCherry* is expressed by a weak promoter, its transcription is extremely low in both the convergent and divergent looped constructs. This suggests that weak promoters are very sensitive to genomic contexts and can be "overwhelmed" by transcription derived from strong promoters.

To systematically test the impact that PSB has on loops containing two highly expressed genes, a GRS site was inserted between them in tandem, convergent, and divergent configuration (Figure 4). GRS had a positive impact on *emGFP* transcription for all three configurations (3.5-fold increase in tandem, 7-fold in convergent, and 2.5-fold in divergent). It also significantly improved the transcription of *mCherry* in the tandem (3-fold) and convergent constructs (2-fold), but only had a moderate impact on the levels of the divergent configuration. For *emGFP*, the transcription trend is tandem > convergent > divergent. This pattern is different than what was observed previously [3]. We believe that the difference can be explained by the fact that the latter study was carried out on a small plasmid rather than on the large chromosome and/or that, in the plasmid study, supercoils can diffuse all along a ~5 kb vector sequence while they are trapped in a 2.5 kb chromosomal topological domain in our study. All together, our work suggests that tandem organization is the optimal configuration for high gene expression. Studies on the natural organization of genes in the bacterial chromosome corroborate this inference [68–70].

The results reported here have permitted us to formulate a comprehensive model that sheds light on how context sensitivity impacts promoter activity. This model is based on a dynamic epigenetic mechanism involving topological barriers like protein-bound DNA loops, genome architecture, and transcriptionally induced PSB (Figure 5). By quantifying the impact that two chromosomal conformations have on context sensitivity, we demonstrated the genome-wide scale of this epigenetic model. It has been well-documented that the genome architecture and transcription profile change dynamically with growth phase, carbon source, and environmental stress in response to changes in the level and activity of different proteins like NAPs. We propose that such changes at a local scale cause genes to be embedded between different topological barriers and to be transcribed in different gene layout contexts, thus epigenetically impacting their transcription. This model explains how the expression of hundreds of genes can be modulated within less than two minutes after environmental changes. It may additionally be enforced by post-translational modifications (phosphorylation, acetylation, etc.) which are highly dynamic and have been shown to modulate protein activities. Our epigenetic model tightly correlates with the findings from L. Serrano's lab [71]. In this work, they reported that a large part of transcriptional regulation is determined by non-canonical factors such as DNA supercoiling and genome organization. The diagram of a simplified genomic region that contains sequences which allow for several proteins to create different DNA loops illustrates how signals controlling these proteins and loop formation would result in the generation of several alternate topological barriers and local gene layouts that would produce very different levels for the "B" transcript (Figure 5). We are now applying these basic concepts to the design of complex genetic programs and synthetic genomes that we are currently engineering within our labs.

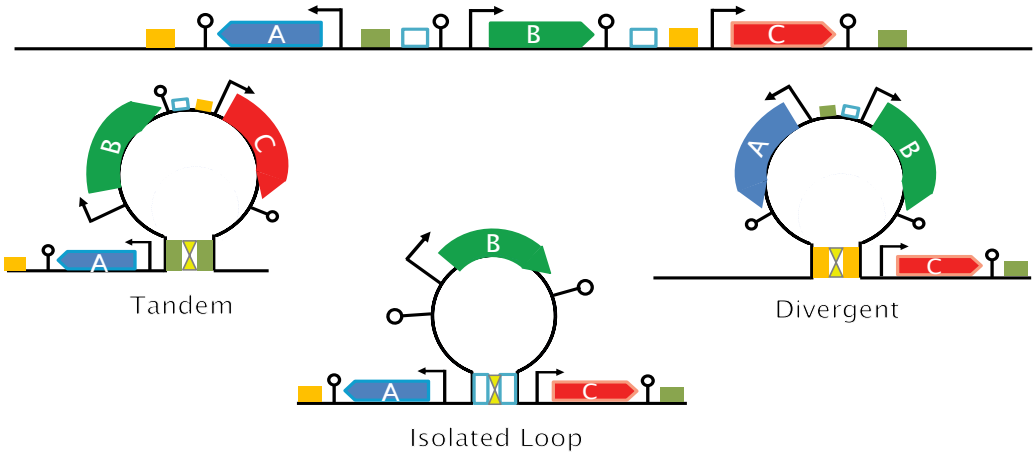

Figure 5. Model of bacterial epigenetic regulation. This diagram illustrates how alternate DNA looping (through the action of different DNA-binding proteins that bridge distant DNA regions) within a genomic domain containing 3 genes (A–C) would be expected to result in different transcription levels for the "B" gene.

5. Conclusions

Our study suggests that context sensitivity is due to inserting genes into uncharacterized DNA loops containing a variable number of transcription units. It is proposed to depend on several factors operating within the loops: the gene layout, transcription interference, promoter strength, and DNA topology. It also depends on the genomic transcription and architecture dictated by carbon sources. We have additionally demonstrated that a gene can be effectively isolated from context sensitivity by incorporating it within a protein-bound DNA loop structure. The model we have proposed will lead to (i) new fundamental discoveries and advances in synthetic biology and (ii) significant improvements in the design/engineering of synthetic genomes. In a fundamental point of view, this work has highlighted some of the mechanisms that govern epigenetic transcription regulation in bacteria.

Supplementary Materials: The following supporting information can be downloaded at: https://www.mdpi.com/article/10.3390/applmicrobiol5010017/s1, Figure S1: DNA sequences used in the work. Figure S2: Diagram of the transposon vector. Figure S3: Transcription of p1-*emGFP* is not affected by transcriptional read-through. Figure S4: Context sensitivity in 1MB regions flanking *oriC* and *terC* sites. Figure S5: Genetic maps showing the local genomic context of non-mutagenic insertion sites in the Ori and Ter regions. Figure S6: Transcriptomic data in glucose and glycerol at 2.17 to 2.26 MB. Figure S7: Lambda cI expression upon rhamnose induction. Figure S8: Transcription of p3-*emGFP* and p10-*mCherry* (tandem configuration with GRS) in various lambda cI contexts. Figure S9: TPS for non-transcribed (closed boxes) and transcribed (dotted boxes) constructs in looped and un-looped configurations. Table S1: Plasmid list. Table S2: Primer list. Table S3: Strain list. Table S4: Library list. Table S5: T-test on data with loops containing two genes.

Author Contributions: Conceptualization, B.C.J.; methodology, N.S. and B.C.J.; investigation, N.S. and B.C.J.; data curation, N.S., L.J. and B.C.J.; writing—original draft preparation, L.J. and B.C.J.; writing—review and editing, L.J.; supervision, L.J. and B.C.J.; project administration, L.J. and B.C.J. All authors have read and agreed to the published version of the manuscript.

Funding: This study was supported by the EU FP7 project ST-FLOW (n° 289326), and recurring research funds from CNRS (Centre National de la Recherche Scientifique) and UEVE (Université d'Evry Val d'Essonne).

Data Availability Statement: Data are included in this published article (and its additional Supplementary Materials). Raw data for RT-qPCR will be made available upon reasonable request.

Acknowledgments: We thank Noemie Brisemeur, Elodie Roche, Hafez El Sayyed, Romaine Bodiniere, Jogelindo da Veiga Moreira, Morgane Champleboux, and Marko Radojkovic for assistance with construction of strains and RT-qPCR, and Efthymia Lioliou from Synovance for comments that greatly improved the manuscript. We thank François Képès for initiating this work and Costas Bouyioukos for valuable discussions and interpretations of the data. We thank the referees whose comments helped us to consolidate our manuscript.

Conflicts of Interest: Author Brian C. Jester holds shares in the company Synovance. The remaining authors declare that the research was conducted in the absence of any commercial or financial relationships that could be construed as a potential conflict of interest.

References

1. Bryant, J.A.; Sellars, L.E.; Busby, S.J.W.; Lee, D.J. Chromosome Position Effects on Gene Expression in *Escherichia coli* K-12. *Nucleic Acids Res.* **2014**, *42*, 11383–11392. [CrossRef]
2. Scholz, S.A.; Diao, R.; Wolfe, M.B.; Fivenson, E.M.; Lin, X.N.; Freddolino, P.L. High-Resolution Mapping of the *Escherichia coli* Chromosome Reveals Positions of High and Low Transcription. *Cell Syst.* **2019**, *8*, 212–225.e9. [CrossRef] [PubMed]
3. Yeung, E.; Dy, A.J.; Martin, K.B.; Ng, A.H.; Del Vecchio, D.; Beck, J.L.; Collins, J.J.; Murray, R.M. Biophysical Constraints Arising from Compositional Context in Synthetic Gene Networks. *Cell Syst.* **2017**, *5*, 11–24.e12. [CrossRef] [PubMed]
4. Kim, S.; Beltran, B.; Irnov, I.; Jacobs-Wagner, C. Long-Distance Cooperative and Antagonistic RNA Polymerase Dynamics via DNA Supercoiling. *Cell* **2019**, *179*, 106–119.e16. [CrossRef]
5. Johnstone, C.P.; Galloway, K.E. Supercoiling-Mediated Feedback Rapidly Couples and Tunes Transcription. *Cell Rep.* **2022**, *41*, 111492. [CrossRef]
6. Visser, B.J.; Sharma, S.; Chen, P.J.; McMullin, A.B.; Bates, M.L.; Bates, D. Psoralen Mapping Reveals a Bacterial Genome Supercoiling Landscape Dominated by Transcription. *Nucleic Acids Res.* **2022**, *50*, 4436–4449. [CrossRef] [PubMed]
7. Deng, S.; Stein, R.A.; Higgins, N.P. Organization of Supercoil Domains and Their Reorganization by Transcription. *Mol. Microbiol.* **2005**, *57*, 1511–1521. [CrossRef]
8. Dorman, C.J. DNA Supercoiling and Transcription in Bacteria: A Two-Way Street. *BMC Mol. Cell Biol.* **2019**, *20*, 26. [CrossRef]
9. Verma, S.C.; Qian, Z.; Adhya, S.L. Architecture of the *Escherichia coli* Nucleoid. *PLoS Genet.* **2019**, *15*, e1008456. [CrossRef]
10. Killian, J.L.; Ma, J.; Wang, M.D. CHAPTER 3. RNA Polymerase as a Torsional Motor. In *Chemical Biology*; Landick, R., Strick, T., Wang, J., Eds.; Royal Society of Chemistry: Cambridge, UK, 2021; pp. 46–71, ISBN 978-1-78801-365-9.
11. Le Berre, D.; Reverchon, S.; Muskhelishvili, G.; Nasser, W. Relationship between the Chromosome Structural Dynamics and Gene Expression—A Chicken and Egg Dilemma? *Microorganisms* **2022**, *10*, 846. [CrossRef] [PubMed]
12. Hustmyer, C.M.; Landick, R. Bacterial Chromatin Proteins, Transcription, and DNA Topology: Inseparable Partners in the Control of Gene Expression. *Mol. Microbiol.* **2024**, *122*, 81–112. [CrossRef]
13. Liu, L.F.; Wang, J.C. Supercoiling of the DNA Template during Transcription. *Proc. Natl. Acad. Sci. USA* **1987**, *84*, 7024–7027. [CrossRef] [PubMed]
14. Ma, J.; Bai, L.; Wang, M.D. Transcription Under Torsion. *Science* **2013**, *340*, 1580–1583. [CrossRef] [PubMed]
15. Janissen, R.; Barth, R.; Polinder, M.; van der Torre, J.; Dekker, C. Single-Molecule Visualization of Twin-Supercoiled Domains Generated during Transcription. *Nucleic Acids Res.* **2023**, *52*, 1677–1687. [CrossRef]
16. Chong, S.; Chen, C.; Ge, H.; Xie, X.S. Mechanism of Transcriptional Bursting in Bacteria. *Cell* **2014**, *158*, 314–326. [CrossRef]
17. Champoux, J.J. DNA Topoisomerases: Structure, Function, and Mechanism. *Annu. Rev. Biochem.* **2001**, *70*, 369–413. [CrossRef]
18. Chen, S.H.; Chan, N.-L.; Hsieh, T. New Mechanistic and Functional Insights into DNA Topoisomerases. *Annu. Rev. Biochem.* **2013**, *82*, 139–170. [CrossRef]
19. Gellert, M.; Mizuuchi, K.; O'Dea, M.H.; Nash, H.A. DNA Gyrase: An Enzyme That Introduces Superhelical Turns into DNA. *Proc. Natl. Acad. Sci. USA* **1976**, *73*, 3872–3876. [CrossRef]
20. Palma, C.S.D.; Kandavalli, V.; Bahrudeen, M.N.M.; Minoia, M.; Chauhan, V.; Dash, S.; Ribeiro, A.S. Dissecting the in Vivo Dynamics of Transcription Locking Due to Positive Supercoiling Buildup. *Biochim. Biophys. Acta (BBA)—Gene Regul. Mech.* **2020**, *1863*, 194515. [CrossRef] [PubMed]
21. Zechiedrich, E.L.; Khodursky, A.B.; Bachellier, S.; Schneider, R.; Chen, D.; Lilley, D.M.J.; Cozzarelli, N.R. Roles of Topoisomerases in Maintaining Steady-State DNA Supercoiling in *Escherichia coli*. *J. Biol. Chem.* **2000**, *275*, 8103–8113. [CrossRef]
22. Sinden, R.R.; Pettijohn, D.E. Chromosomes in Living *Escherichia coli* Cells Are Segregated into Domains of Supercoiling. *Proc. Natl. Acad. Sci. USA* **1981**, *78*, 224–228. [CrossRef] [PubMed]
23. Postow, L.; Hardy, C.D.; Arsuaga, J.; Cozzarelli, N.R. Topological Domain Structure of the *Escherichia coli* Chromosome. *Genes. Dev.* **2004**, *18*, 1766–1779. [CrossRef] [PubMed]

24. Deng, S.; Stein, R.A.; Higgins, N.P. Transcription-Induced Barriers to Supercoil Diffusion in the *Salmonella typhimurium* Chromosome. *Proc. Natl. Acad. Sci. USA* **2004**, *101*, 3398–3403. [CrossRef] [PubMed]
25. Bignaud, A.; Cockram, C.; Borde, C.; Groseille, J.; Allemand, E.; Thierry, A.; Marbouty, M.; Mozziconacci, J.; Espéli, O.; Koszul, R. Transcription-Induced Domains Form the Elementary Constraining Building Blocks of Bacterial Chromosomes. *Nat. Struct. Mol. Biol.* **2024**, *31*, 489–497. [CrossRef] [PubMed]
26. Leng, F.; McMacken, R. Potent Stimulation of Transcription-Coupled DNA Supercoiling by Sequence-Specific DNA-Binding Proteins. *Proc. Natl. Acad. Sci. USA* **2002**, *99*, 9139–9144. [CrossRef] [PubMed]
27. Leng, F.; Chen, B.; Dunlap, D.D. Dividing a Supercoiled DNA Molecule into Two Independent Topological Domains. *Proc. Natl. Acad. Sci. USA* **2011**, *108*, 19973–19978. [CrossRef]
28. Dages, S.; Zhi, X.; Leng, F. Fis Protein Forms DNA Topological Barriers to Confine Transcription-coupled DNA Supercoiling in *Escherichia coli*. *FEBS Lett.* **2020**, *594*, 791–798. [CrossRef]
29. Strick, T.R.; Allemand, J.-F.; Bensimon, D.; Bensimon, A.; Croquette, V. The Elasticity of a Single Supercoiled DNA Molecule. *Science* **1996**, *271*, 1835–1837. [CrossRef] [PubMed]
30. Forth, S.; Deufel, C.; Sheinin, M.Y.; Daniels, B.; Sethna, J.P.; Wang, M.D. Abrupt Buckling Transition Observed during the Plectoneme Formation of Individual DNA Molecules. *Phys. Rev. Lett.* **2008**, *100*, 148301. [CrossRef]
31. Berger, M.; Gerganova, V.; Berger, P.; Rapiteanu, R.; Lisicovas, V.; Dobrindt, U. Genes on a Wire: The Nucleoid-Associated Protein HU Insulates Transcription Units in *Escherichia coli*. *Sci. Rep.* **2016**, *6*, 31512. [CrossRef]
32. Watson, G.D.; Chan, E.W.; Leake, M.C.; Noy, A. Structural Interplay between DNA-Shape Protein Recognition and Supercoiling: The Case of IHF. *Comput. Struct. Biotechnol. J.* **2022**, *20*, 5264–5274. [CrossRef] [PubMed]
33. Fulcrand, G.; Dages, S.; Zhi, X.; Chapagain, P.; Gerstman, B.S.; Dunlap, D.; Leng, F. DNA Supercoiling, a Critical Signal Regulating the Basal Expression of the Lac Operon in *Escherichia coli*. *Sci. Rep.* **2016**, *6*, 19243. [CrossRef] [PubMed]
34. Yan, Y.; Ding, Y.; Leng, F.; Dunlap, D.; Finzi, L. Protein-Mediated Loops in Supercoiled DNA Create Large Topological Domains. *Nucleic Acids Res.* **2018**, *46*, 4417–4424. [CrossRef]
35. Japaridze, A.; Yang, W.; Dekker, C.; Nasser, W.; Muskhelishvili, G. DNA Sequence-Directed Cooperation between Nucleoid-Associated Proteins. *iScience* **2021**, *24*, 102408. [CrossRef]
36. Boulas, I.; Bruno, L.; Rimsky, S.; Espeli, O.; Junier, I.; Rivoire, O. Assessing in Vivo the Impact of Gene Context on Transcription through DNA Supercoiling. *Nucleic Acids Res.* **2023**, *51*, 9509–9521. [CrossRef]
37. Mutalik, V.K.; Guimaraes, J.C.; Cambray, G.; Lam, C.; Christoffersen, M.J.; Mai, Q.-A.; Tran, A.B.; Paull, M.; Keasling, J.D.; Arkin, A.P.; et al. Precise and Reliable Gene Expression via Standard Transcription and Translation Initiation Elements. *Nat. Methods* **2013**, *10*, 354–360. [CrossRef]
38. Cambray, G.; Guimaraes, J.C.; Mutalik, V.K.; Lam, C.; Mai, Q.-A.; Thimmaiah, T.; Carothers, J.M.; Arkin, A.P.; Endy, D. Measurement and Modeling of Intrinsic Transcription Terminators. *Nucleic Acids Res.* **2013**, *41*, 5139–5148. [CrossRef]
39. Yarnell, W.S.; Roberts, J.W. Mechanism of Intrinsic Transcription Termination and Antitermination. *Science* **1999**, *284*, 611–615. [CrossRef]
40. Oram, M.; Pato, M.L. Mu-Like Prophage Strong Gyrase Site Sequences: Analysis of Properties Required for Promoting Efficient Mu DNA Replication. *J. Bacteriol.* **2004**, *186*, 4575–4584. [CrossRef]
41. Rossignol, M.; Basset, A.; Espéli, O.; Boccard, F. NKBOR, a Mini-Tn10-Based Transposon for Random Insertion in the Chromosome of Gram-Negative Bacteria and the Rapid Recovery of Sequences Flanking the Insertion Sites in *Escherichia coli*. *Res. Microbiol.* **2001**, *152*, 481–485. [CrossRef]
42. Kuhlman, T.E.; Cox, E.C. Site-Specific Chromosomal Integration of Large Synthetic Constructs. *Nucleic Acids Res.* **2010**, *38*, e92. [CrossRef]
43. Kuhlman, T.E.; Cox, E.C. A Place for Everything: Chromosomal Integration of Large Constructs. *Bioeng. Bugs* **2010**, *1*, 298–301. [CrossRef]
44. Keseler, I.M.; Mackie, A.; Santos-Zavaleta, A.; Billington, R.; Bonavides-Martínez, C.; Caspi, R.; Fulcher, C.; Gama-Castro, S.; Kothari, A.; Krummenacker, M.; et al. The EcoCyc Database: Reflecting New Knowledge about *Escherichia coli* K-12. *Nucleic Acids Res.* **2017**, *45*, D543–D550. [CrossRef]
45. Calculations: Converting from Nanograms to Copy Number. Available online: https://eu.idtdna.com/pages/education/decoded/article/calculations-converting-from-nanograms-to-copy-number (accessed on 5 February 2025).
46. How Many mRNAs Are in a Cell? Available online: https://book.bionumbers.org/how-many-mrnas-are-in-a-cell/ (accessed on 6 February 2025).
47. Nicolas, P.; Mäder, U.; Dervyn, E.; Rochat, T.; Leduc, A.; Pigeonneau, N.; Bidnenko, E.; Marchadier, E.; Hoebeke, M.; Aymerich, S.; et al. Condition-Dependent Transcriptome Reveals High-Level Regulatory Architecture in *Bacillus subtilis*. *Science* **2012**, *335*, 1103–1106. [CrossRef]
48. Kim, J.; Oliveros, J.C.; Nikel, P.I.; De Lorenzo, V.; Silva-Rocha, R. Transcriptomic Fingerprinting of P*seudomonas putida* under Alternative Physiological Regimes. *Environ. Microbiol. Rep.* **2013**, *5*, 883–891. [CrossRef]

49. Chen, Z.; Li, Q.; Zhou, P.; Li, B.; Zhao, Z. Transcriptome Sequencing Reveals Key Metabolic Pathways for the Synthesis of L-Serine from Glycerol and Glucose in *Escherichia coli*. *Biochem. Eng. J.* **2023**, *191*, 108804. [CrossRef]
50. Lamoureux, C.R.; Decker, K.T.; Sastry, A.V.; Rychel, K.; Gao, Y.; McConn, J.L.; Zielinski, D.C.; Palsson, B.O. A Multi-Scale Expression and Regulation Knowledge Base for *Escherichia coli*. *Nucleic Acids Res.* **2023**, *51*, 10176–10193. [CrossRef]
51. Scholz, S.A.; Lindeboom, C.D.; Freddolino, P.L. Genetic Context Effects Can Override Canonical *Cis* Regulatory Elements in *Escherichia coli*. *Nucleic Acids Res.* **2022**, *50*, 10360–10375. [CrossRef]
52. Stokke, C.; Flåtten, I.; Skarstad, K. An Easy-To-Use Simulation Program Demonstrates Variations in Bacterial Cell Cycle Parameters Depending on Medium and Temperature. *PLoS ONE* **2012**, *7*, e30981. [CrossRef]
53. Bremer, H.; Dennis, P.P. Transition Period Following a Nutritional Shift-up in the Bacterium *Escherichia coli* B/R: Stable RNA and Protein Synthesis. *J. Theor. Biol.* **1975**, *52*, 365–382. [CrossRef]
54. Helmstetter, C.E. Timing of Synthetic Activities in the Cell Cycle. In *Escherichia coli and Salmonella: Cellular and Molecular Biology*; ASM Press: Washington, DC, USA, 1996; pp. 1627–1639.
55. Mercier, R.; Petit, M.-A.; Schbath, S.; Robin, S.; El Karoui, M.; Boccard, F.; Espéli, O. The MatP/matS Site-Specific System Organizes the Terminus Region of the *E. coli* Chromosome into a Macrodomain. *Cell* **2008**, *135*, 475–485. [CrossRef]
56. Valens, M.; Thiel, A.; Boccard, F. The MaoP/maoS Site-Specific System Organizes the Ori Region of the *E. coli* Chromosome into a Macrodomain. *PLoS Genet.* **2016**, *12*, e1006309. [CrossRef]
57. Liu, M.; Durfee, T.; Cabrera, J.E.; Zhao, K.; Jin, D.J.; Blattner, F.R. Global Transcriptional Programs Reveal a Carbon Source Foraging Strategy by *Escherichia coli*. *J. Biol. Chem.* **2005**, *280*, 15921–15927. [CrossRef]
58. Oehler, S.; Müller-Hill, B. High Local Concentration: A Fundamental Strategy of Life. *J. Mol. Biol.* **2010**, *395*, 242–253. [CrossRef]
59. Révet, B.; Von Wilcken-Bergmann, B.; Bessert, H.; Barker, A.; Müller-Hill, B. Four Dimers of λ Repressor Bound to Two Suitably Spaced Pairs of λ Operators Form Octamers and DNA Loops over Large Distances. *Curr. Biol.* **1999**, *9*, 151–154. [CrossRef]
60. Dodd, I.B.; Perkins, A.J.; Tsemitsidis, D.; Egan, J.B. Octamerization of λ CI Repressor Is Needed for Effective Repression of P_{RM} and Efficient Switching from Lysogeny. *Genes. Dev.* **2001**, *15*, 3013–3022. [CrossRef] [PubMed]
61. Dodd, I.B.; Shearwin, K.E.; Perkins, A.J.; Burr, T.; Hochschild, A.; Egan, J.B. Cooperativity in Long-Range Gene Regulation by the λ CI Repressor. *Genes. Dev.* **2004**, *18*, 344–354. [CrossRef]
62. Ding, Y.; Manzo, C.; Fulcrand, G.; Leng, F.; Dunlap, D.; Finzi, L. DNA Supercoiling: A Regulatory Signal for the λ Repressor. *Proc. Natl. Acad. Sci. USA* **2014**, *111*, 15402–15407. [CrossRef]
63. Meyer, S.; Reverchon, S.; Nasser, W.; Muskhelishvili, G. Chromosomal Organization of Transcription: In a Nutshell. *Curr. Genet.* **2018**, *64*, 555–565. [CrossRef]
64. Nagy-Staron, A.; Tomasek, K.; Caruso Carter, C.; Sonnleitner, E.; Kavčič, B.; Paixão, T.; Guet, C.C. Local Genetic Context Shapes the Function of a Gene Regulatory Network. *eLife* **2021**, *10*, e65993. [CrossRef]
65. Burz, D.S.; Ackers, G.K. Single-Site Mutations in the C-Terminal Domain of Bacteriophage.Lambda. cI Repressor Alter Cooperative Interactions between Dimers Adjacently Bound to OR. *Biochemistry* **1994**, *33*, 8406–8416. [CrossRef]
66. Hao, N.; Palmer, A.C.; Ahlgren-Berg, A.; Shearwin, K.E.; Dodd, I.B. The Role of Repressor Kinetics in Relief of Transcriptional Interference between Convergent Promoters. *Nucleic Acids Res.* **2016**, *44*, 6625–6638. [CrossRef] [PubMed]
67. Cho, B.-K.; Zengler, K.; Qiu, Y.; Park, Y.S.; Knight, E.M.; Barrett, C.L.; Gao, Y.; Palsson, B.Ø. The Transcription Unit Architecture of the *Escherichia coli* Genome. *Nat. Biotechnol.* **2009**, *27*, 1043–1049. [CrossRef]
68. Jeong, K.S.; Ahn, J.; Khodursky, A.B. Spatial Patterns of Transcriptional Activity in the Chromosome of *Escherichia coli*. *Genome Biol.* **2004**, *5*, R86. [CrossRef]
69. Képès, F.; Jester, B.C.; Lepage, T.; Rafiei, N.; Rosu, B.; Junier, I. The Layout of a Bacterial Genome. *FEBS Lett.* **2012**, *586*, 2043–2048. [CrossRef] [PubMed]
70. Junier, I.; Rivoire, O. Conserved Units of Co-Expression in Bacterial Genomes: An Evolutionary Insight into Transcriptional Regulation. *PLoS ONE* **2016**, *11*, e0155740. [CrossRef] [PubMed]
71. Yus, E.; Lloréns-Rico, V.; Martínez, S.; Gallo, C.; Eilers, H.; Blötz, C.; Stülke, J.; Lluch-Senar, M.; Serrano, L. Determination of the Gene Regulatory Network of a Genome-Reduced Bacterium Highlights Alternative Regulation Independent of Transcription Factors. *Cell Syst.* **2019**, *9*, 143–158.e13. [CrossRef]